Please cite this article in press as: Tonelli et al., Dual inhibition of MAPK/ERK and BMP signaling induces entorhinal-like identity in mouse ESC-derived pallial progenitors, Stem Cell Reports (2024), https://doi.org/10.1016/j.stemcr.2024.12.002

Stem Cell Reports
Article
ISSCR
OPEN ACCESS

Dual inhibition of MAPK/ERK and BMP signaling induces entorhinal-like identity in mouse ESC-derived pallial progenitors

Fabrizio Tonelli,[1] Ludovico Iannello,[2] Stefano Gustincich,[3] Angelo Di Garbo,[2,4] Luca Pandolfini,[3,5,*] and Federico Cremisi[1,2,5,6,*]

[1]Laboratorio di Biologia, Scuola Normale Superiore, 56126 Pisa, Italy
[2]Istituto di Biofisica, Consiglio Nazionale delle Ricerche, 56124 Pisa, Italy
[3]Center for Human Technologies, Central RNA Lab, Istituto Italiano di Tecnologia, 16152 Genova, Italy
[4]Dipartimento di Fisica, Università di Pisa, 56127 Pisa, Italy
[5]These authors contributed equally
[6]Lead contact
*Correspondence: luca.pandolfini@iit.it (L.P.), federico.cremisi@sns.it (F.C.)
https://doi.org/10.1016/j.stemcr.2024.12.002

SUMMARY

The mechanisms that determine distinct embryonic pallial identities remain elusive. The central role of Wnt signaling in directing dorsal telencephalic progenitors to the isocortex or hippocampus has been elucidated. Here, we show that timely inhibition of MAPK/ERK and BMP signaling in neuralized mouse embryonic stem cells (ESCs) specifies a cell identity characteristic of the allocortex. Comparison of the global gene expression profiles of neural cells generated by MAPK/ERK and BMP inhibition (MiBi cells) with those of cells from early postnatal encephalic regions reveals a pallial identity of MiBi cells, distinct from isocortical and hippocampal cells. MiBi cells display a unique pattern of gene expression and connectivity, and share molecular and electrophysiological features with the entorhinal cortex. Our results suggest that early changes in cell signaling can specify distinct pallial fates that are maintained by specific neuronal lineages independent of subsequent embryonic morphogenetic interactions and can determine their functional connectivity.

INTRODUCTION

Neuralization of mouse embryonic stem cells (mESCs) and human induced pluripotent stem cells (hiPSCs) has been instrumental in elucidating the general mechanisms underlying cortical cell specification (Kelava and Lancaster, 2016; Qian et al., 2020). However, dissecting the mechanisms of precise specification of distinct pallial region identities remains a challenge.

The major pallial regions comprising 90% and 10% of the human cortex, respectively, are the six-layer isocortex (IsC) and the allocortex (Creutzfeldt, 1995), the latter of which can be subdivided into distinct areas based on cytoarchitectural, functional, and evolutionary classifications (Zilles, 2004). The involvement of extracellular signaling in the commitment and patterning of dorsal telencephalic precursors was dissected in neuralizing mESCs and hiPSCs. Activation of MAPK/ERK signaling in a narrow time window of differentiation, corresponding to the *in vivo* time of specification of the anterior-posterior axis of the IsC, can induce rostral markers of cortical arealization in neural progenitor cells (NPCs) derived from both mESCs and hiPSCs (Imaizumi et al., 2018; Terrigno et al., 2018a). Wnt signaling is critical for directing dorsal telencephalic progenitors toward a dentate gyrus hippocampal fate (Terrigno et al., 2018b; Yu et al., 2014). Hippocampal NPCs derived from hiPSCs can be differentiated into CA3 neurons *in vitro* (Sarkar et al., 2018), or maintained as progenitors in an *in vitro* hippocampal stem niche containing Wnt signaling and laminin 511 (Dunville et al., 2022). However, although isocortical and hippocampal patterning have been extensively studied, little is known about the development and acquisition of the different pallial identities that ultimately allow the brain to function as a whole. Here, we show that (1) simultaneous MAPK/ERK and BMP inhibition during a narrow time interval is sufficient to specify an allocortical identity similar to that of the entorhinal cortex (EnC) and (2) that this fate is maintained *in vitro* until full maturation of electrically active neurons. Surprisingly, dual MAPK/ERK and BMP inhibited cells develop global gene expression profiles, connectivity, and electrical activity patterns in adherent cultures that are distinct from cells with hippocampal and cortical identities and more similar to EnC cells. Collectively, our results suggest that the acquisition of distinct pallial fates and connectivity patterns at later stages of development may be specified and regulated by pathway activity during early cortical patterning and appears to be largely unaffected by subsequent interactions with other cell types. Finally, we have shown that homotypic neuronal cultures develop unique network electrophysiological activity over time, but the repertoire of these activity patterns can be modified and expanded when different neuronal circuits are assembled *in vitro*.

Please cite this article in press as: Tonelli et al., Dual inhibition of MAPK/ERK and BMP signaling induces entorhinal-like identity in mouse ESC-derived pallial progenitors, Stem Cell Reports (2024), https://doi.org/10.1016/j.stemcr.2024.12.002

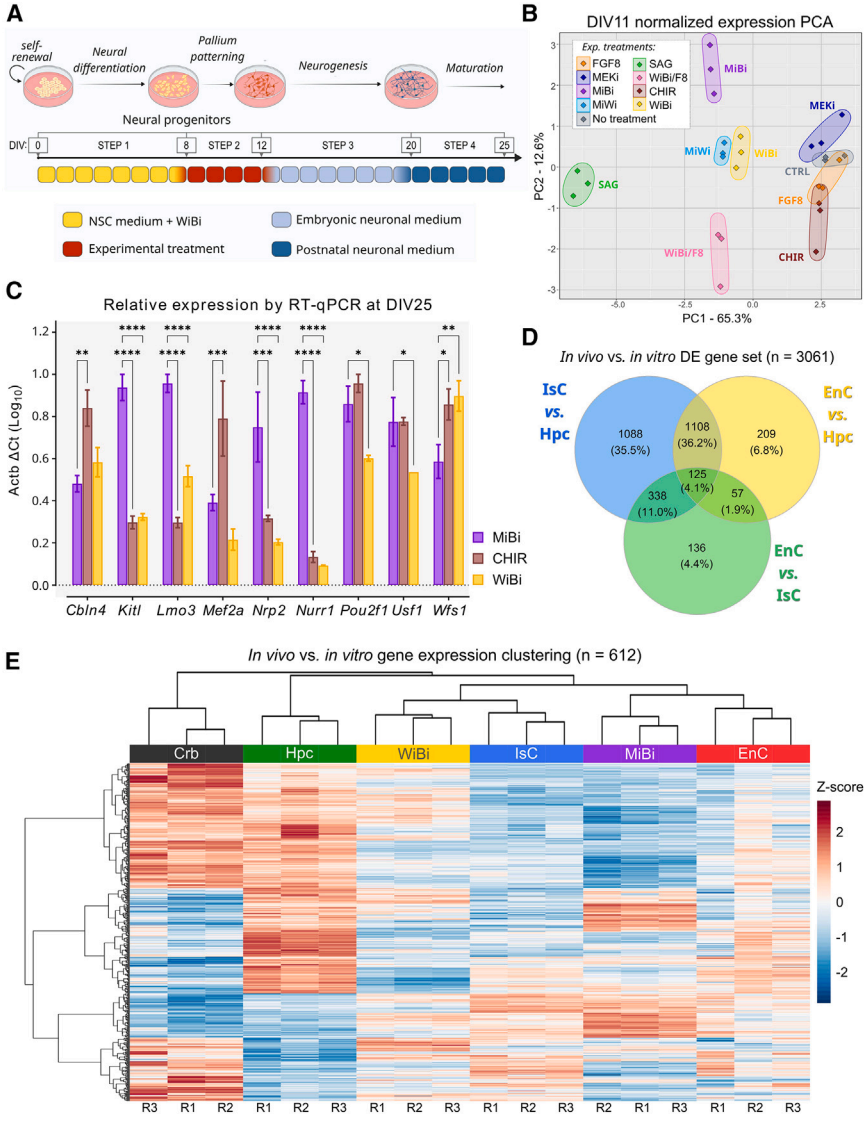

Figure 1. Inhibition of MAPK/ERK and BMP signaling induces pallial identity distinct from isocortical and hippocampal identity

(A) mESC differentiation protocol. Differentiation media included different combinations of treatments listed in (B) (see text for explanation of acronyms and Methods for composition). NSC, neural stem cell.

(B) PCA of the expression levels of 12 early pallial and extra-pallial markers evaluated by quantitative reverse-transcription PCR (RT-qPCR) in the different cultures at DIV11 (see Table S1; Figure S1A; $n = 3$ independent experiments). PC1 and PC2 are shown with their relative variance percentages, mimicking the dorsal-ventral (right to left) and rostral-caudal (bottom to top) brain axes.

(C) RT-qPCR analysis of allocortex and entorhinal markers in DIV25 cultures ($n = 3$ independent experiments). Mean ± SEM is shown; only comparisons against MiBi are shown; two-way ANOVA, Dunnett's multiple comparison test; *p value < 0.05, **p value < 0.01, ***p value < 0.001, ****p value < 0.0001.

(D) Venn diagram of differentially expressed (DE) genes between entorhinal cortex (EnC), hippocampus (Hpc), and isocortex (IsC), selected for "*in vivo* vs. *in vitro*" analysis.

(E) Hierarchical clustering of samples and gene expression levels that account for PCs 2 and 3 of the PCA shown in Figure S1G. R1, R2, and R3 denote replicates. The heatmap scale indicates the normalized Z score gene expression level.

RESULTS

Timely inhibition of MAPK/ERK and BMP signaling induces a gene expression profile typical of allocortex

We induced telencephalic neuralization of mESCs by Wnt/BMB inhibition (with 53AH and LDN193189: WiBi) from day *in vitro* (DIV) 0 to DIV7 (Figure 1A). At DIV8, telencephalic NPCs can be further specified toward either an isocortical or hippocampal identity by prolonged Wnt/BMP inhibition, or by Wnt reactivation (with CHIR99021: CHIR), respectively (Terrigno et al., 2018b). During early development, activation/inhibition of key signaling pathways establishes morphogen gradients that pattern the brain along the embryonic axes (frontal-caudal, dorsal-ventral, and medial-lateral; Puelles et al., 2019). In particular, fibroblast growth factor (FGF) signaling plays a critical role in pallial frontal-caudal patterning by antagonizing the expression of the caudal patterning transcription factor COUP-TF1 (*Nr2f1*), which in turn specifies entorhinal identity when overexpressed during early corticogenesis (Feng et al., 2021). Therefore, to identify the molecular determinants of caudal allocortex identity, we examined the effects of MAPK/ERK (MEK) signaling inhibition, which antagonizes FGF signaling by suppressing the expression of frontal markers and supporting the pallial expression of COUP-TFI (Terrigno et al., 2018a). We compared the effects of MEK inhibition with the effects of manipulating other signaling pathways (Wnt, BMP, Shh, and FGF) in the time window between DIV8 and DIV11. We examined the expression of early forebrain markers at DIV11, an *in vitro* time point

Please cite this article in press as: Tonelli et al., Dual inhibition of MAPK/ERK and BMP signaling induces entorhinal-like identity in mouse ESC-derived pallial progenitors, Stem Cell Reports (2024), https://doi.org/10.1016/j.stemcr.2024.12.002

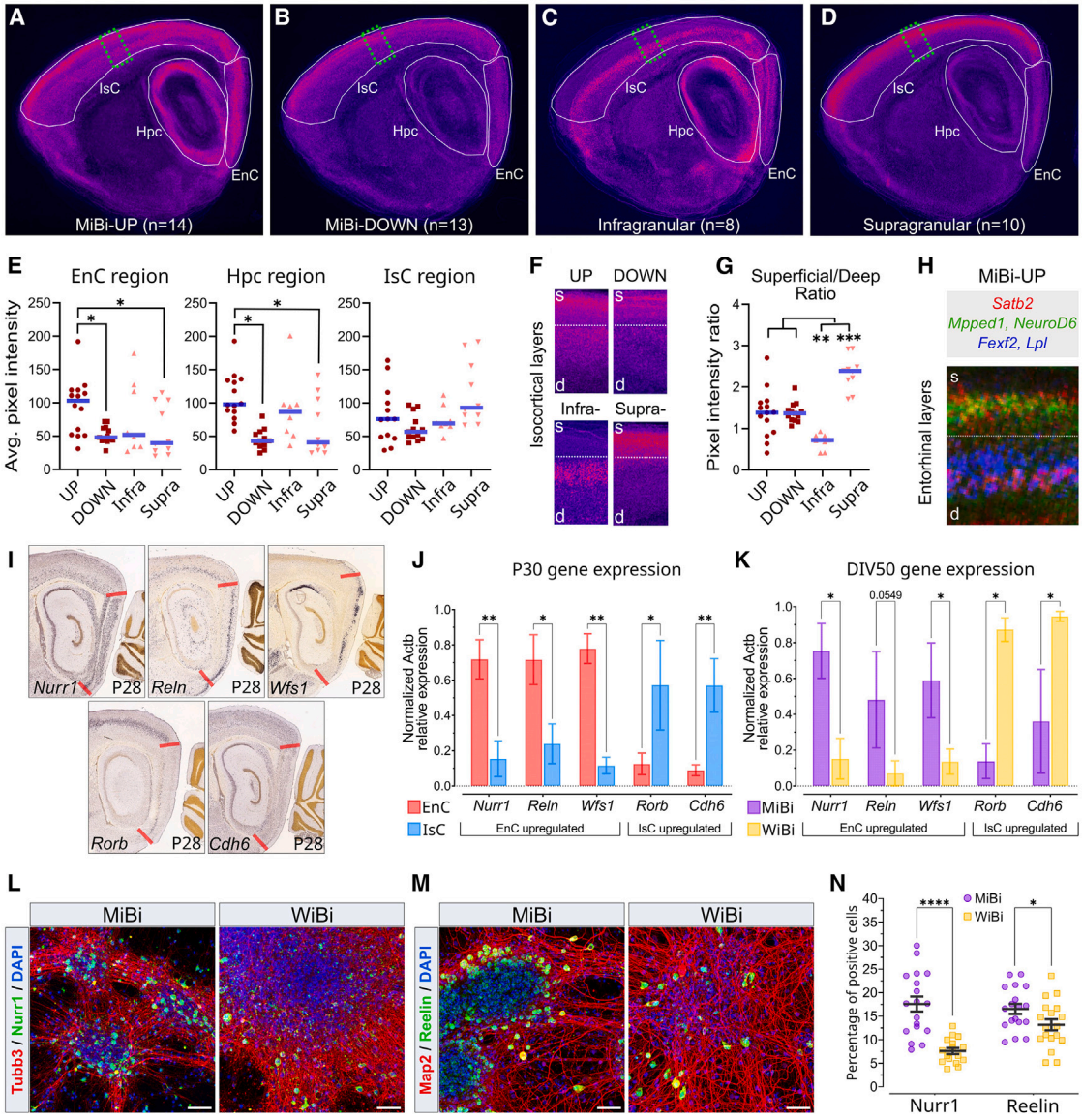

Figure 2. MiBi neurons express markers of entorhinal cortex identity

(A–D) Virtual *in situ* hybridizations (ISHs) of sagittal mouse brain sections at P4. Cumulative expression levels of DE genes in MiBi vs. WiBi cells (A and B) and markers of infra- and supragranular neurons (C and D) show distinct expression patterns in IsC, Hpc, and EnC (*n* = number of genes).

(E) Quantification of signal from individual ISH images superimposed in (A–D). Symbols indicate the pixel intensity value of a single ISH image, bars indicate the mean; Kruskal-Wallis test, **p* value < 0.05.

(F) Enlargements of green-dashed areas in cortical regions of (A–D) showing superficial (s) and deep (d) layer expression of DE genes in MiBi vs. WiBi cells (UP, DOWN) and between infra- and supragranular layers (Infra-, Supra-).

(G) Quantification of signal from individual ISH images superimposed in (F). Symbols indicate the ratio of pixel intensity value between superficial and deep layer expression of each ISH image, bars indicate the mean; Kruskal-Wallis test, **q < 0.01, ***q < 0.001.

(H) ISH overlay of MiBi vs. WiBi upregulated genes with specific expression patterns in EnC layers.

(I) ISH images of P28 mouse brain sections from the Allen Brain Map showing the expression patterns of entorhinal (*Nurr1*, *Reln*, and *Wfs1*) and isocortical (*Rorb* and *Cdh6*) markers. Thick red lines delineate the EnC.

(J and K) RT-qPCR analysis of markers shown in (I) *in vivo* or *in vitro* (for *in vivo* comparison, brain regions were dissected from *n* = 4 mice; for *in vitro* comparison, *n* = 3 independent experiments). Mean ± SEM is shown for both comparisons; two-way ANOVA followed by the Benjamini, Krieger, and Yekutieli two-step linear step-up procedure for correction of multiple testing. Unless otherwise indicated, **p* value < 0.05, ***p* value < 0.01.

(legend continued on next page)

comparable to the mid-embryonic stage (Terrigno et al., 2018a). Principal component analysis (PCA) of the expression levels of 12 markers differentially expressed in early embryonic pallial regions (Table S1) revealed that only 4 treatments generated cells with a distinct molecular identity compared to isocortical (WiBi) and hippocampal (CHIR) cultures: Shh activation (SAG), WiBi plus FGF8 activation (WiBi/F8), MEK/Wnt inhibition (MiWi), and MEK/BMP inhibition (MiBi; Figures 1B and S1A). Specifically, PCA differentiated cultures by mimicking the orientation of developmental axes in the embryonic brain. Principal component 1 (PC1), which accounted for most of the variance (65.3%), differentiated cultures characterized by activation of the Shh pathway (SAG, Figure 1B, left) and expression of ventral pallium identity genes (*Dlx2*, *CoupTFI*, and *Lmo3*) from cultures expressing hippocampal and isocortical markers (Figure 1B, right) such as *Emx2*, *Pax6*, *Lhx2*, and *Foxg1* (Figure S1A). Conversely, PC2 (12.6%) appeared to distinguish the caudal-rostral identity of the pallium, as cultures characterized by inhibition or activation of the FGF pathway (upper and lower halves, respectively; Figure 1B) are spatially segregated. Consistent with these observations, SAG and WiBi/F8 treatments specify subpallial structures and anterior isocortical neurons, respectively (Cederquist et al., 2019; Imaizumi et al., 2018; Kim et al., 2014; Terrigno et al., 2018a). Moreover, the identity of MiWi cells appeared to be very similar to that of WiBi cells in the PCA. Therefore, we focused on MiBi treatment, which was able to induce a more pronounced caudal cortical cell identity in NPCs (Figures 1B and S1A). This finding aligns with studies showing that FGF signaling activation antagonizes the transcriptional machinery supporting early caudal cortical development (Borello et al., 2008; Faedo et al., 2008; Feng et al., 2021). Given the caudal pallial identity of MiBi cells, we analyzed the expression of selected markers of more differentiated allocortex and EnC neurons at a later stage (DIV25) of *in vitro* differentiation (Abellán et al., 2014; Feng et al., 2021; Puelles et al., 2019; Ramsden et al., 2015) These genes showed enrichment upon MiBi treatment compared to CHIR (*Kitl*, *Lmo3*, *Nrp2*, and *Nr4a2*) and to an even greater extent compared to WiBi (*Kitl*, *Lmo3*, *Nrp2*, *Nr4a2*, *Pou2f1*, and *Usf1*; Figure 1C). These results indicate that MiBi cells are different from WiBi and CHIR cells and suggest that they share an allocortical identity with CHIR cells.

To better investigate the pallial identity of MiBi cultures, we compared DIV25 WiBi and MiBi cells with IsC, hippocampus (Hpc), cerebellum, and EnC from mice at post-natal day 5, (P5), a developmentally comparable time point as suggested by previous observations (Gaspard et al., 2008). The P5 EnC and IsC showed the lowest degree of global gene expression difference (n = 656 differentially expressed [DE] genes, 4.4% of total gene number), followed by the EnC vs. Hpc comparison (n = 1,499 DE genes, 10.1% of total gene number, Figure S1B). As pointed out in a recent study (Franjic et al., 2020), these findings may be due to both the similarity of the laminar structure present in both EnC and IsC, with deep-layer isocortical excitatory neurons well represented in EnC layers, and the marked heterogeneity observed within hippocampal subregions. We selected the DE genes among the three cortical regions (IsC, Hpc, and EnC, n = 3061) to reduce the complexity of the transcriptomic data and to analyze the components of the PCA that account for the positional cellular identities of the *in vitro* and *in vivo* samples (Figures 1D and S1C–S1E; see Methods). The first and second principal components (PC1 and 2) discriminated between *in vivo* and *in vitro* samples (Figure S1F), while the second and third components (PC2 and 3), accounting for 36.1% of the total variance, distinguished the expression profiles of different culture conditions and brain regions (Figure S1G). Hierarchical clustering of genes accounting for most of the variance of PC2 and 3 (see Methods) revealed the presence of 3 gene clusters (Figure S1H) involved in the regulation of different biological processes (Figure S1I). This gene set highlighted a significant similarity between MiBi and EnC samples, which differed from WiBi and IsC (Figure 1E). Taken together, these observations suggest that MiBi cells have a pallial identity similar to that of EnC.

MiBi cells exhibit a molecular identity and axonogenesis program similar to an entorhinal-like identity

To further characterize the molecular identity and neuronal types of MiBi cells, we focused on the DE genes (absolute $\log_2$ fold change $\geq$ 2) that distinguished MiBi and WiBi cultures. We analyzed the average spatial expression patterns of those genes showing cortical expression at P5 in the Allen Brain Map *in situ* hybridization (ISH) repository (https://developingmouse.brain-map.org/). The number of upregulated (MiBi-UP) and downregulated (MiBi-DOWN) genes in MiBi cells available for this analysis was 14 and 13, respectively (Figure S2A; Table S2). Some MiBi-UP genes showed a clear enrichment in EnC compared to IsC (*Crym*, *Hcn1*, *Nos1*, and *Pcsk2*), while others were expressed in both regions (*Fezf2* and *Satb2*; Figure S2A). We performed semi-quantification of MiBi-UP and MiBi-DOWN gene expression in the available ISH images (Figures 2A, 2B, and 2E). Overall,

(L and M) Immunofluorescence (IF) of MiBi and WiBi cells with Nurr1 and Tubb3 antibodies (green and red staining in L) or Reelin and Map2 antibodies (green and red staining in M); DAPI is shown as blue staining in (L) and (M).
(N) Quantification of IF-positive cells in cultures as in (L) and (M) (n = 3 independent experiments). Mean ± SEM is shown; unpaired t test followed by Holm-Šídák correction for multiple comparisons; *p value < 0.05, ****p value < 0.0001.

Please cite this article in press as: Tonelli et al., Dual inhibition of MAPK/ERK and BMP signaling induces entorhinal-like identity in mouse ESC-derived pallial progenitors, Stem Cell Reports (2024), https://doi.org/10.1016/j.stemcr.2024.12.002

MiBi-UP genes were preferentially upregulated in EnC and Hpc and showed differential expression compared to MiBi-DOWN genes (Figure 2E). However, the expression of MiBi-UP and MiBi-DOWN genes did not differ in IsC (Figure 2E), making the enrichment of MiBi-UP genes in EnC alone insufficient to conclusively suggest an entorhinal-like identity of MiBi cells. To gain further insight into the specificity of MiBi-WiBi DE genes, we compared their expression with that of markers of supra- and infragranular isocortical neurons (Figures 2C and 2D; Table S2; Lodato and Arlotta, 2015). We found 8 infragranular and 10 supragranular genes with robust signal in the Allen Brain Map ISH repository (Figure S2A). In both EnC and Hpc, MiBi-UP genes showed significantly higher expression levels compared to MiBi-DOWN genes and supragranular markers (Figure 2E), whereas no significant variation in expression levels was observed in IsC or compared to infragranular markers. Thus, MiBi-UP genes were generally upregulated in both EnC and Hpc, while downregulated in supragranular layers, with some exceptions. For example, *Satb2*, a MiBi-UP gene, is a supragranular marker and is not upregulated in EnC. Finally, MiBi-UP and MiBi-DOWN genes showed no statistical difference in the ratio of superficial to deep layer markers (Superficial/Deep Ratio) in the isocortical layers (Figures 2F and 2G), although some of them showed a clear specific expression in the EnC layers (Figure 2H). Taken together, these observations suggest that MiBi cells have an identity distinct from WiBi cells but similar to that of EnC cells, although the upregulation in MiBi cultures of genes such as *Satb2* and *Fezf2*, which are expressed *in vivo* in both EnC and IsC, could be interpreted as incomplete conversion to an EnC identity or the acquisition of another pallial identity. An alternative hypothesis is that early MiBi and WiBi cultures at DIV25 may show a different degree of cell differentiation.

To further investigate the nature of MiBi cells, we analyzed the expression of EnC and IsC markers at a later stage of *in vitro* neuronal differentiation (DIV50) and compared their expression levels with P30 brain regions. We found that genuine markers of EnC (*Nurr1* and *Wls1*) and IsC (*Rorb* and *Cdh6*; Figures 2I and 2J) are upregulated in MiBi and WiBi cells, respectively (Figures 2K, 2L, and 2N). Furthermore, layer II of the rodent EnC is characterized by the presence of a mixture of excitatory pyramidal neurons and large multipolar neurons, the latter known as stellate cells (SCs) or fan cells (FCs) in the medial and lateral EnC, respectively (Witter et al., 2017). Reelin, a marker of EnC SCs/FCs, is expressed in a higher proportion of MiBi cells compared to WiBi cultures (Figures 2M and 2N), supporting the notion of an enhanced entorhinal-like identity of MiBi cultures. We then tested whether MiBi treatment could activate a program of SC differentiation using an SC-specific reporter. We generated a lentiviral GFP reporter construct under the control of the SC-specific enhancer MEC-13-53A of the Teneurin-3 (*Tenm3*) gene (Figure S2G; Nair et al., 2020), which encodes a transsynaptic transmembrane protein involved in the establishment of the entorhinal-hippocampal circuit (Berns et al., 2018). Transduced MiBi cultures showed a significantly higher proportion of cells expressing the GFP reporter compared to other pallial and extrapallial cultures (Figures S2H and S2I). This observation is consistent with the higher proportion of cells expressing Reelin protein in MiBi cultures (Figures 2M and 2N), suggesting that MiBi treatment may support the differentiation of SCs.

To understand the mechanisms involved in the specification of MiBi cells and EnC cells, we analyzed the Biological Process Gene Ontology (GO) of their DE gene sets derived from both *in vitro* (MiBi vs. WiBi) and *in vivo* (EnC vs. IsC) comparisons. The genes upregulated *in vitro* and *in vivo* shared 9 of the 20 most enriched GO terms, while no common terms were found among the genes downregulated (Figures S3A and S3B). Genes belonging to the common upregulated GO terms were pooled into a unique dataset (Table S3), on which a pairwise similarity matrix based on gene overlap from the biological processes was generated to create a network plot. The resulting enrichment map of the MiBi/EnC common terms (Figure 3A) showed 4 clusters grouping similar processes. We then focused on the three most enriched terms, namely axonogenesis, positive regulation of cell projection organization, and regulation of membrane potential. The gene-concept network depicting the gene linkage within the three terms showed that 84.4% of them were also MiBi upregulated genes (yellow dots against gray in Figure 3B; total number of genes = 307; Table S4). These latter observations suggest that MiBi cells share a distinct gene expression profile with the EnC that is specifically associated with the control of neuronal connectivity. Altogether, our data indicate that MiBi treatment is capable of generating *in vitro* neuronal cultures that resemble *bona fide* EnC neurons.

MiBi and WiBi neurons show different connectivity patterns

The EnC and Hpc can develop unique circuit connectivity that reflects important higher animal functions such as memory-guided and goal-directed navigation (Issa et al., 2024; Malone et al., 2024; Nilssen et al., 2019). We wondered whether we could observe a difference in terms of cellular connectivity in our cultures. Adherent CHIR, WiBi, and MiBi cultures matured synaptic connections with PSD95-positive spines at DIV30, and the spine density was comparable among the three different culture types (Figure S4).

To compare the connectivity of MiBi and WiBi neurons, we tested their ability to generate long-range projections and form heterotypic connections. To this end, we

Please cite this article in press as: Tonelli et al., Dual inhibition of MAPK/ERK and BMP signaling induces entorhinal-like identity in mouse ESC-derived pallial progenitors, Stem Cell Reports (2024), https://doi.org/10.1016/j.stemcr.2024.12.002

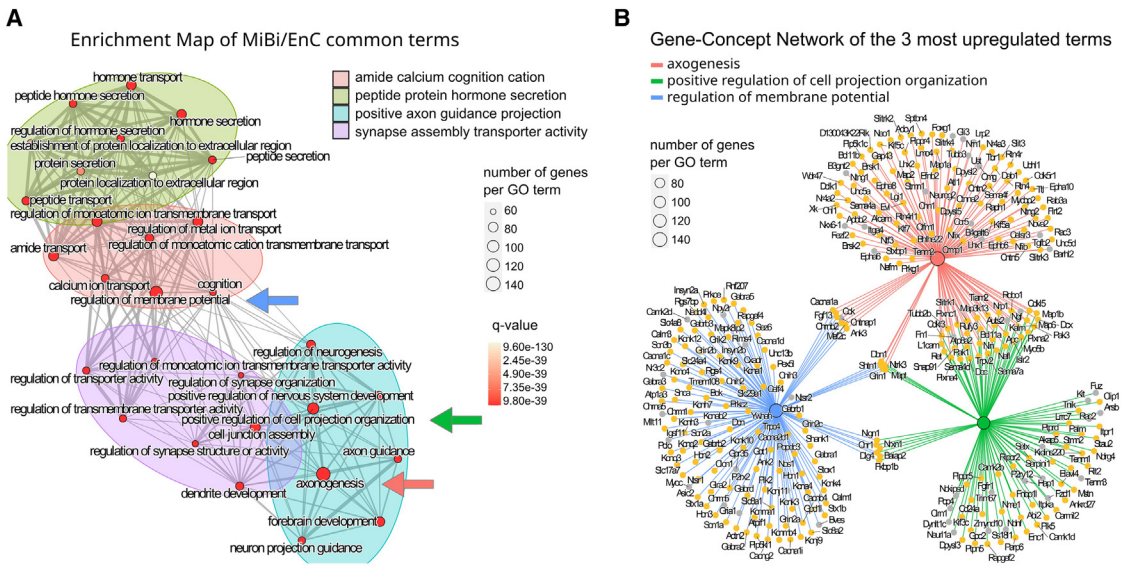

Figure 3. MiBi neurons share with EnC neurons the activation of genes involved in axonogenesis and cell identity

(A) Enrichment map of common upregulated GO terms between MiBi and EnC (see Figure S3A). Terms common to MiBi vs. WiBi and EnC vs. IsC were analyzed as described (see Methods). The dot size indicates the number of genes belonging to that ontology, while the color scale indicates the false discovery rate value. The degree of similarity is proportional to the thickness of the links (shown in gray). Clusters, which group GO terms based on similarity, are color-coded.

(B) Gene concept network of the three most enriched terms from (A) (colored arrows). Yellow dots indicate MiBi upregulated genes, while gray dots indicate genes that are not DE. Categories are color-coded, and the dot size of the categories refers to the number of genes belonging to that ontology.

developed an *in vitro* connectivity assay in which adherent cultures were seeded 500 μm apart on glass bottom dishes using a cross-shaped 4-well insert (see Methods), and we measured the ability of virally labeled MiBi and WiBi neurons to send processes to either surrounding unlabeled WiBi or CHIR cultures (Figures 4A–4E and S5). After 10 days in co-culture, mCherry-tagged WiBi cell processes efficiently crossed the 500 μm gap and reached both WiBi and CHIR untagged cultures (Figure 4B, insets D1 and 2). However, the majority of WiBi processes that reached CHIR cells tended to bend and failed to establish deep contacts in the culture (arrows in Figure 4B, inset D2), in contrast to those that invaded homotypic cultures (Figure 4B, inset D1). EGFP-tagged MiBi cell processes, on the contrary, successfully invaded WiBi and CHIR untagged cultures with comparable efficiency (Figure 4C, insets D3 and 4). We quantified the total number and length of fiber branches as well as the average branching and tortuosity of fibers generated by WiBi or MiBi virally labeled cells within CHIR and WiBi unlabeled cultures (Figures 4E–4I, S5B, and S5C). This analysis was performed in defined areas of the unlabeled cultures, opposite the labeled cultures and away from the center where fibers from all cultures converge (Figures S5A–S5C; see Methods). The total branch length of WiBi or MiBi neurons within WiBi cultures was comparable, while the total branch length of WiBi within CHIR cultures was significantly lower than that of MiBi cells (Figure 4F), confirming the different affinity of WiBi and MiBi axons for CHIR cultures. WiBi processes within CHIR also showed the lowest number of branches among the comparisons, while surprisingly, MiBi processes within WiBi cultures showed the highest number (Figure 4G). However, the latter observation is consistent with the average branch length and tortuosity index of WiBi fibers, indicating that they preferentially navigate straighter within WiBi cultures than MiBi processes, avoiding CHIR cells (Figures 4H and 4I). Conversely, MiBi processes showed no significant differences in average branch length and tortuosity index within CHIR or WiBi cultures, indicating a clear difference in axon pathfinding of MiBi and WiBi neurons (Figures 4H and 4I). Based on GO analysis, the enrichment of genes involved in axonogenesis and cell projection shown by MiBi cultures suggests that MiBi neurons exhibit more robust axonal growth compared to WiBi neurons, which may contribute to the deeper projection in CHIR cultures. To test this hypothesis, we examined the normalized ratio of the density of labeled neuronal processes in unlabeled hippocampal cultures compared to unlabeled isocortical cultures, calculated individually for both MiBi and WiBi cultures. This value is not affected by the absolute axonal growth rate of the fibers and indicates the propensity of a process to extend within one of the two cultures. This analysis revealed that

Please cite this article in press as: Tonelli et al., Dual inhibition of MAPK/ERK and BMP signaling induces entorhinal-like identity in mouse ESC-derived pallial progenitors, Stem Cell Reports (2024), https://doi.org/10.1016/j.stemcr.2024.12.002

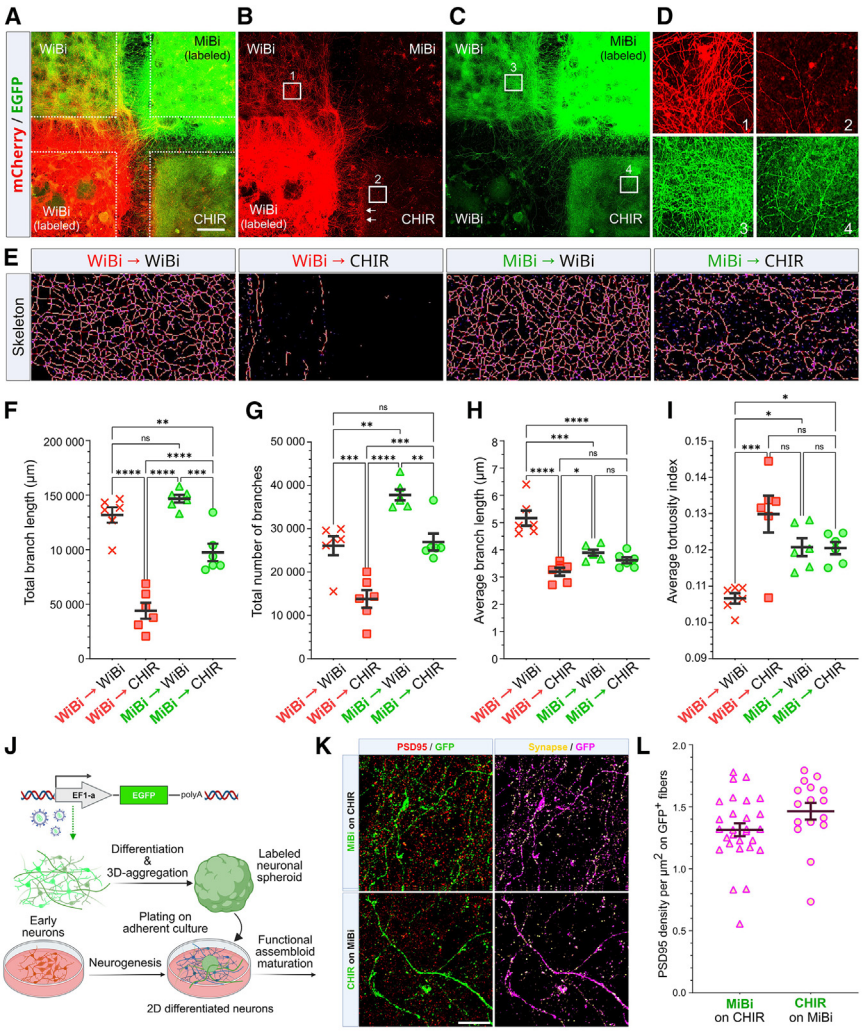

Figure 4. Connectivity of *in vitro* cultures

(A–D) Connectivity assay.

(A) Representative image of DIV30 cultures labeled with EGFP (MiBi, upper right) or mCherry (WiBi, lower left) lentiviral vectors, seeded together with unlabeled CHIR (lower right) and WiBi (upper left) cultures in quadripartite culture inserts at DIV18 (see Methods; scale bar: 500 µm).

(B and C) Same as in (A), highlighting the contribution of WiBi (B) or MiBi (C) fiber connectivity.

(D) Enlargements of the areas numbered in (B) and (D).

(E) Magnification of example regions used for quantification and pattern analysis of EGFP and mCherry fibers (see Methods). Tagged skeletons of segmented cell processes are pseudo-colored to highlight network branches.

(F–I) Quantification of connectivity and fiber parameters. Measurements are averages of regions as shown in Figure S4 (n = 3 independent experiments). In each plot, mean ± SEM is shown; one-way ANOVA, Tukey multiple comparison test; *p-value <0.05, **p value < 0.01, ***p value < 0.001, ****p value < 0.0001; ns, not significant.

(J) Schematic of a functional assembloid (FA) with fibers (green) connecting to the underlying adherent culture. FAs were generated by aggregates of DIV18 cells (spheroids) labeled with EGFP lentivector and seeded onto an adherent isochronic culture (see Methods for details).

(K) Magnification of spheroid fibers in adherent culture stained for GFP and PSD95. The synapses of the spheroid fibers were visualized by considering the positive pixels for PSD95 and GFP (yellow) and then overlaying them with GFP (magenta, see Methods; scale bar: 25 µm).

(L) Synapse quantification was performed considering positive pixels as in (K). Synapses were measured in terms of density of GFP-positive area covered by synapses. Comparisons between images acquired from MiBi/CHIR and CHIR/MiBi FA showed no statistical differences in terms of synapses density (n = 4 independent experiments; 2-tailed t test, p value = 0.0879).

MiBi processes were significantly longer than WiBi processes within CHIR cultures (Figures S5D and S5E), although the relative proportion of elongated processes did not appear to vary between cultures (Figure S5F). Therefore, these results confirm that the observed differences in cell connectivity between MiBi and WiBi cultures are largely due to the presence of specific molecular properties that regulate the different axonal affinity, rather than the axonal growth rate of MiBi and WiBi cells.

Having shown that MiBi neuronal processes can explore and contact CHIR cells in adherent cultures, we investigated whether this ability could also be maintained by cell aggregates (spheroids). We found that functional assembloids (FAs) could be formed when spheroids of DIV20 neurons were seeded onto adherent isochronic cultures (Figure 4J; see Methods). We plated virally labeled MiBi spheroids onto adherent CHIR cultures (MiBi/CHIR) or vice versa (CHIR/MiBi) and assessed the number of PSD95-positive spines contacting fluorescent processes extending from the aggregates (Figure 4K). Spheroid fibers were associated with multiple PSD95-positive puncta in both MiBi/CHIR and CHIR/MiBi FAs, with no significant difference in the degree of connectivity between them (Figure 4L).

WiBi, CHIR, and MiBi neuronal cultures develop distinct patterns of network activity

Primary cortical neurons cultured in adherence generate neuronal networks that exhibit complex patterns of

Please cite this article in press as: Tonelli et al., Dual inhibition of MAPK/ERK and BMP signaling induces entorhinal-like identity in mouse ESC-derived pallial progenitors, Stem Cell Reports (2024), https://doi.org/10.1016/j.stemcr.2024.12.002

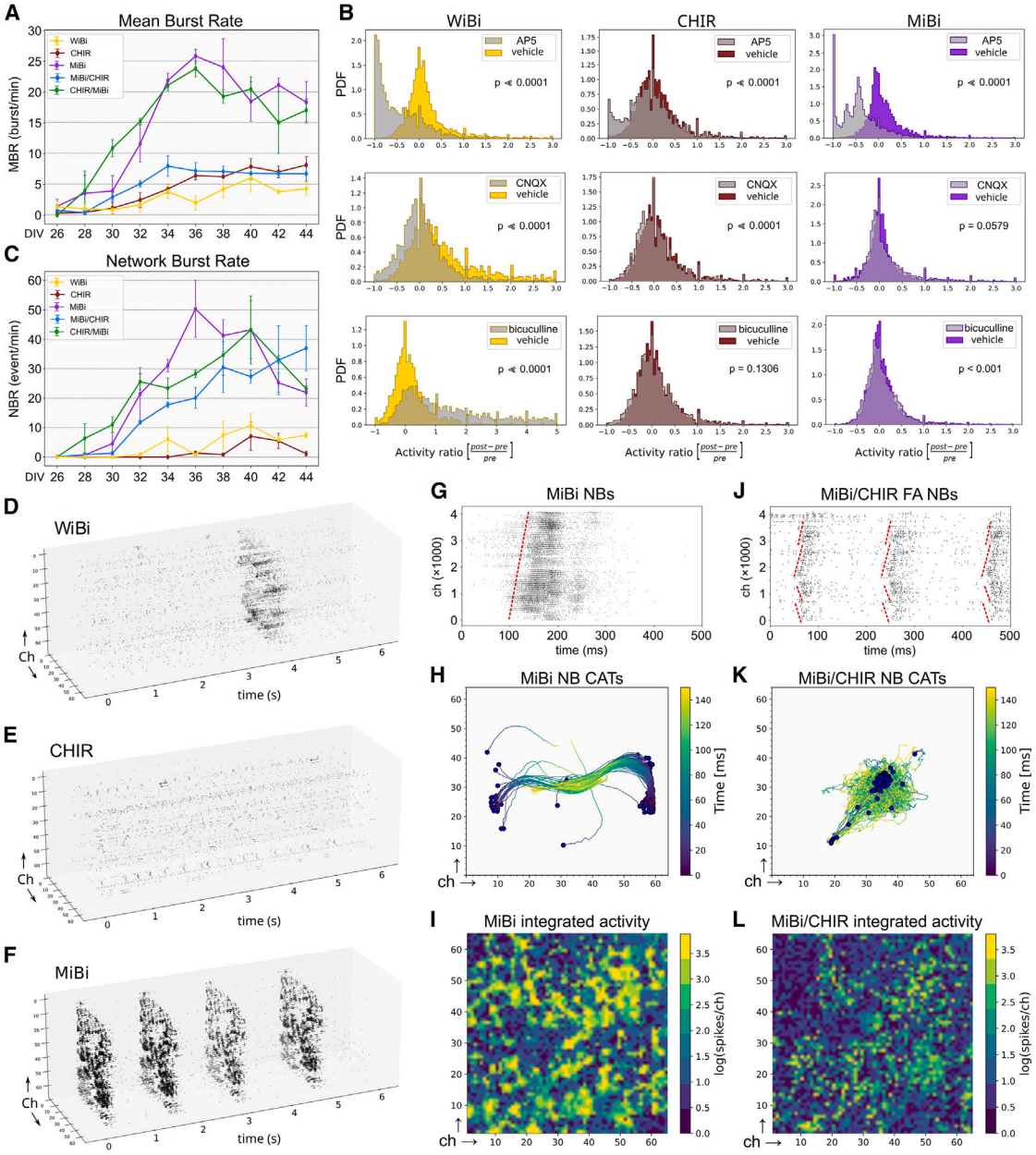

Figure 5. Electrophysiological and network activity of *in vitro* cultures

(A) Time trend of MBR in single channels (mean ± SEM).

(B) Probability distribution of the variation of the activity of each channel before and after drug administration at DIV44. The colored distributions represent the variation of baseline activity (without drugs) considering different time portions of spontaneous activity. The gray distributions represent the variation after drug administration. A non-parametric Mann-Whitney U test was performed to determine statistically significant differences between the baseline and post-drug distributions. *p* values (p) < 0.01 were considered significant. PDF, probability density function.

(C) Time trend of NBR in all cultures (mean ± SEM). In (A), (B) and (C), $n \geq 2$ independent experiments.

(D–F) Reconstructed 3D raster plots of a short time window in pure cultures, preserving the spatial position of the channels.

(G and J) Representative 2D raster plots of MiBi and MiBi/CHIR FA showing a time delay in NB propagation across the chip (red dashed lines).

(legend continued on next page)

activity (Charlesworth et al., 2015; Dias et al., 2021). However, differences in activity patterns related to the identity of cultured neurons have not been fully investigated. Using a high-density microelectrode array (HD-MEA) with 4,096 channels, we were able to longitudinally compare a number of activity parameters of pure cultures and FAs (Videos S1 and S2). In particular, we evaluated the mean firing rate (MFR) in single channels, the mean burst duration (MBD), and the mean burst frequency (MBR) of neuronal spikes, as well as the network burst rate (NBR), the center of activity trajectories (CATs) of network bursts (NBs), and the functional connectivity.

Sorting of the distinct spike waveforms recorded from each active channel showed that all cultures had a similar distribution of clusters per channel and that 95%–99% of the channels were associated with 1–4 units (Figure S6A), making analysis of a single channel representative of very small local circuits. MFR, MBR, and MBD increased from the earliest time point (DIV26) to the final time point of analysis (DIV44) in all cultures, demonstrating progressive functional maturation of the networks (Figures 5A, S6B, and S6C; Video S1). To determine the contribution of excitatory and inhibitory inputs to the observed activity patterns, we examined the effect of selective antagonists of ionotropic glutamate and GABA receptors in cultures at DIV44. While the MFR of WiBi and CHIR cells responded to CNQX (AMPA and kainate antagonist) and AP5 (NMDA antagonist) with a higher proportion of channels inhibited by AP5, the MFR of MiBi cells was only significantly affected by AP5 (Figure 5B). In contrast, the MBR was significantly reduced by either AP5 (Figures S6D and S6E) or CNQX (Figures S6F and S6G) in both WiBi (Figures S6D and S6F) and MiBi (Figures S6E and S6G) cultures. Notably, AP5 decreased the MBR of MiBi cells and completely abolished that of WiBi cells (Figures S6D and S6E), indicating a key role of NMDA receptors in the generation of burst activity. Furthermore, AP5 exerted a stronger inhibition on WiBi and MiBi cells than on CHIR cells (Figure 5B). Finally, only WiBi and MiBi cultures showed a significant increase in activity after exposure to bicuculline ($GABA_A$ antagonist; Figure 5B). Taken together, these data indicate that after 20 days of maturation (DIV44), the activity of the three cultures was driven by glutamatergic neurons that manifested NMDA-dependent plasticity and that only WiBi and MiBi cultures were sensitive to GABAergic inhibition.

Starting from DIV40, NBs spread throughout the network in WiBi cultures (see Methods; Figures 5C and 5D), whereas they were rarely observed in CHIR cultures (Figures 5C and 5E). Interestingly, MiBi cultures started to generate NBs earlier, at DIV32 and at a higher frequency than WiBi cultures (Figures 5C, 5F, S6I, and S6K). To test whether different levels of neuronal maturation were involved in the timing of the onset of NB activity between MiBi and WiBi cultures, we monitored the expression of *Egr1* and *Fos*, two genes involved in neuronal plasticity and considered good markers of functionally mature neurons (Minatohara et al., 2016), during the maturation of long-term cultures (DIV25–50). *Egr1* was never differentially expressed between MiBi and WiBi cultures, whereas *Fos* expression fluctuated significantly between DIV25 and DIV35 and then became almost comparable in the two cell types at DIV50 (Figure S6H). This observation suggests that neuronal maturation may not be a primary factor in the onset of NB activity in WiBi and MiBi cells and implies that differences in the onset and pattern of network activity between cultures are mainly determined by their neuronal identity.

The ability of spheroids and adherent cultures to form synaptically connected FAs (Figures 4K and 4L) allowed us to examine the influence of one type of neuronal culture on the activity of another. With the goal of modeling *in vitro* some of the features of the connectivity between the EnC and Hpc, we focused on the connectivity between CHIR and MiBi neurons in FAs. Consistent with the *in vivo* observation that afferent fibers from the EnC influence and guide the establishment of synchronous hippocampal activity (Donato et al., 2017; Shipkov et al., 2024; Valeeva et al., 2019), we observed that the innate tendency of MiBi neurons to generate high-frequency NBs was transferred to CHIR adherent cultures in MiBi/CHIR FAs (Figures 5C–5G, 5J, S6, S6J, S6K, and S6L). Conversely, CHIR spheroids did not affect the rate of NBs of MiBi neurons in CHIR/MiBi FAs at the end of maturation (DIV44, Figure 5C), although their NB patterning was different from that of adherent CHIR and MiBi cultures (Figures S6J, S6K, and S6M; Videos S1 and S2).

To evaluate the dynamics of signal propagation, we performed a CAT analysis for each NB to determine the onset of the synchronization event (see Methods). The onset of each NB occurred in distinct regions of the MiBi and WiBi culture networks, with CATs moving toward the center of the network in less than 150 ms (Figures 5H, 5I, and S6N). Indeed, burst onset times along adjacent channels appeared to be separated by temporal increments

(H and K) CAT plots representative of MiBi and MiBi/CHIR FA. Each blue dot represents the physical center of mass of the activity where the NB starts, while the colored line represents its own trajectory. When the whole network is activated, its center of mass is at the physical center of the chip. The colored scale represents time (ms).
(I and L) Heatmap of network activity in full recording, where each pixel represents an MEA channel, colored according to the log of the number of spikes it recorded.

Please cite this article in press as: Tonelli et al., Dual inhibition of MAPK/ERK and BMP signaling induces entorhinal-like identity in mouse ESC-derived pallial progenitors, Stem Cell Reports (2024), https://doi.org/10.1016/j.stemcr.2024.12.002

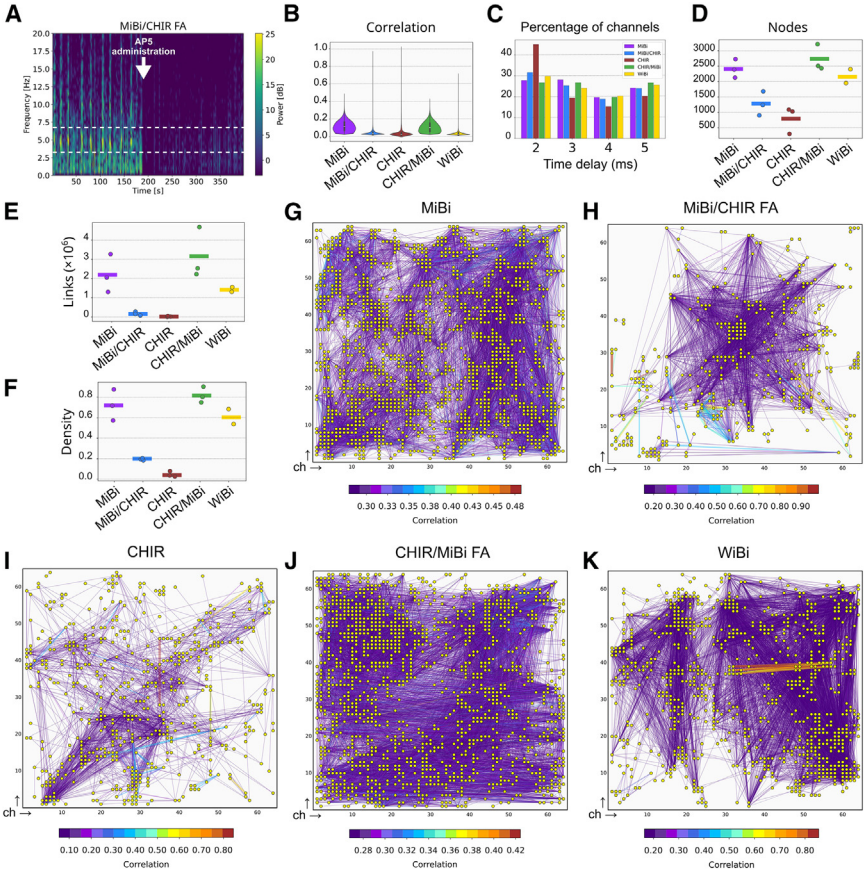

Figure 6. Characterization of network connectivity

(A) Spectrogram analysis of representative firing rate activity (MFR, considering a time bin of 5 ms) for the recording of a MiBi/CHIR FA culture, showing strong theta power during NB activity. Theta power was suppressed by infusion of the NMDA receptor antagonist AP5 (white arrow). Dashed white lines include the frequency range of theta oscillation.

(B) Violin plots of significant correlations (see Methods) for each culture.

(C) Distribution of the time delay between two spikes of different first and second-order channels, obtained from the connectivity analysis. Each histogram corresponds to the percentage of channels showing a specific time-delay value.

(D) Mean number of nodes of the obtained connectivity graph for each replicate of the different culture.

(E) Average number of links for each culture replicate.

(F) Mean value of network density for each culture replicate. The colored bars are the mean values of the different replicates of the same culture. In (B)–(F), $n \geq 2$ independent experiments.

(G–K) Connectivity plots of representative neuronal cultures. Each yellow point represents an active channel (only 0.5% of nodes with highest correlation are shown); colored lines represent the correlation strength between two points. The color bar indicates the correlation index.

consistent with synaptic connectivity orders (tens of ms across the chip; see dashed red lines in raster plots, Figure 5G). This observation also characterized both CHIR/MiBi and MiBi/CHIR FAs, although in the latter case, the activity of CHIR neurons was driven by MiBi spheroid afferents (Figures 5J and S6O). Accordingly, in MiBi/CHIR FAs, the activity centers were concentrated close to the contact between MiBi spheroids and CHIR culture (Figure 5K), but the NBs also covered channels in the periphery of the HD-MEA (Figures 5J and 5L). We thus conclude that CHIR neurons present beneath the spheroid are responsible for most of the NB activity recorded in MiBi/CHIR FAs. Notably, MiBi/CHIR FAs showed the very same NB activity of MiBi cells, while NB activity of CHIR cells was almost not detectable (Figures 5C–5E, 5F, and S6J–S6L). In addition, MiBi/CHIR FAs alternated between waves of activity in which NBs were more abundant than MiBi NBs and waves of NB inactivity, whereas NBs are quite continuous in MiBi cultures (Figures S6K and S6M), indicating two different types of network activity. Notably, MiBi spheroid-induced activity in CHIR neurons showed periods of NBs with a theta frequency peaking at 5.1 and 5.2 Hz in 2 of the 3 FAs analyzed (Figures 6A and S6P). Periods of theta activity ranged from a few seconds to tens of seconds during NB activity and were sensitive to AP5, which completely abolished NBs (Figure 6A). In contrast to MiBi/CHIR FAs, CHIR cells alone did not show theta frequency oscillations in their firing activity (Figure S6Q). Interestingly, theta activity is induced in hippocampal CA1 both *in vivo* and in cultured brain slices by the main entorhinal excitatory inputs through the perforant/temporoammonic (PP/TA) pathway and is inhibited by AP5 perfusion of EnC, highlighting the importance of entorhinal NMDA receptors in inducing theta generation in hippocampal neurons (Gu and Yakel, 2017; Gu et al., 2017). Furthermore, AP5 is not effective when perfused in HpC and, in our study, affects CHIR neurons to a lesser extent than MiBi neurons (Figure 5B). Based on these observations, we speculate that the activity of MiBi fibers may play a role similar to that of the entorhinal PP/TA pathway in inducing theta activity and that MiBi/CHIR FAs may model some of the functional aspects of EnC-HpC connectivity *in vitro*.

Finally, we assessed network connectivity by analyzing the correlation of channel spike instants at DIV44 and considering a time window of 2–5 ms around the event, which is an estimation of the synaptic delay of first- and second-order

Please cite this article in press as: Tonelli et al., Dual inhibition of MAPK/ERK and BMP signaling induces entorhinal-like identity in mouse ESC-derived pallial progenitors, Stem Cell Reports (2024), https://doi.org/10.1016/j.stemcr.2024.12.002

connectivity (Figure 6B; Sabatini and Regehr, 1999). Using a correlation threshold based on the distribution of correlations of shuffled spike trains (see Methods), the connectivity of network activity was assessed for the channels of the different cultures. The resulting time delay distribution confirmed first- and second-order connectivity (Figure 6C). We found different average numbers of nodes, links, and graph densities (Figures 6D–6F), indicating distinct patterns of network complexity (Figures 6G–6K). Specifically, MiBi and CHIR networks (Figures 6G and 6I) showed the highest and lowest values of node number, links, and density, respectively (Figures 6D–6F), while WiBi networks (Figure 6K) showed intermediate values. MiBi/CHIR and CHIR/MiBi FAs (Figures 6H and 6J) were very similar to their corresponding single culture (CHIR and MiBi, respectively) in terms of number of nodes, links, and graph density. MiBi/CHIR FAs showed a slightly higher network density and number of nodes than CHIR cultures (Figures 6D–6F, 6H, and 6I), but these values were much smaller compared to those of MiBi cultures. Collectively, we conclude that local network connectivity in neurons is intrinsically driven by a developmental program initiated by their commitment to different positional fates through Wnt, BMP, and MEK signaling. Further interactions between different networks may ultimately refine their innate patterns of activity.

DISCUSSION

Dual inhibition of MAPK/ERK and BMP signaling in a narrow time window (MiBi) induced a stable change in the differentiation trajectory of mESC-derived NPCs. MiBi cells expressed markers of the dorsal anterior telencephalon consistent with cell types distinct from hippocampal and isocortical cells. Three observations support the hypothesis that MiBi cells have an entorhinal-like identity: (1) the preferential expression of MiBi upregulated genes in the EnC, (2) the ability of MiBi cells to activate the *Tenm3* promoter, which is particularly active in entorhinal SCs (Nair et al., 2020), and (3) the similarity of the global gene expression profile of MiBi cells to that of early postnatal EnC cells.

The processes of MiBi neurons could contact both isocortical (WiBi) and hippocampal (CHIR) cultures, in contrast to isocortical neurons that explicitly preferred to connect to homotypic cultures over hippocampal cultures. This is reminiscent of the connectivity of the EnC *in vivo*, which serves as a proxy station for processes and signals flowing from the IsC to the Hpc and vice versa (Nilssen et al., 2019; Witter et al., 2017).

Unexpectedly, WiBi, CHIR, and MiBi adherent cultures developed different patterns of electrical activity. In particular, the spontaneous activity of MiBi neurons is remarkably pronounced, with a much higher NBR compared to WiBi, suggesting a role for them in *de novo* formation and shaping of neuronal networks. Neurons in the superficial layers of the developing medial EnC are involved in the neuronal and network maturation of the entorhinal-hippocampal circuit, both through the action of specific neuronal types and through intrinsic prolonged bursting activity (Donato et al., 2017; Griguoli and Cherubini, 2017; Sheroziya et al., 2009).

Interestingly, the interaction between MiBi and CHIR neurons on HD-MEA influenced the activity of the CHIR network, indicating the ability of MiBi/CHIR FAs to form functional connections *in vitro*. Notably, the changes in CHIR network activity induced by MiBi spheroids are reminiscent of the synchronization of entorhinal and hippocampal activity in the early postnatal period (Shipkov et al., 2024; Valeeva et al., 2019), suggesting that an endogenous activity pattern dictated by EnC neurons may control such synchronization (Gu et al., 2017; Leprince et al., 2023). However, these differences are unlikely to be driven by changes in the cell density of the CHIR network, which is little affected by MiBi spheroids in FAs compared to MiBi. Therefore, we hypothesize that functional interactions between different types of neuronal networks can alter their respective spontaneous activity patterns without affecting the connectivity of local networks.

Collectively, our results suggest that timely changes in Wnt, BMP, and MAPK/ERK signaling in early NPCs are sufficient to specify distinct types of pallial identities that are maintained in the absence of subsequent morphogenetic interactions and generate distinct patterns of connectivity and electrical activity.

EXPERIMENTAL PROCEDURES

Mouse ESCs were differentiated into cortical fates using a four-step protocol. Cells were cultured in chemically defined minimal medium with Wnt/BMP inhibitors (WiBi) and reseeded onto poly-ornithine/laminin-coated surfaces. Specific cortical subtypes were induced with combinations of Wnt agonist (53AH) and BMP and MEK inhibitors (LDN193189 hydrochloride and PD0325901). From DIV20, neurons were conditioned with Neurobasal-A medium containing BDNF.

For connectivity assays, neurons were transduced with fluorescent reporters, seeded in precoated silicone wells, and cultured for 10 days. Neuronal spheroids were formed in low-attachment wells, transferred to adherent cultures to form FAs, and further cultured.

Electrophysiological recordings were performed using high-density CMOS-based 4096 microelectrode arrays (Accura, 3Brain) to analyze spiking, bursting, and network synchronization. Drug response and functional connectivity were assessed using custom Python codes. Spike sorting and network analysis were based on PCA and cross-correlation methods.

Detailed descriptions of all experimental procedures are provided in the Methods section of the supplemental information.

RESOURCE AVAILABILITY

Lead contact

Further information and requests for resources and reagents should be directed to and will be fulfilled by the lead contact, Federico Cremisi (federico.cremisi@sns.it).

Materials availability

This study did not generate new unique reagents. However, any questions about reagents or animals used can be directed to the lead contact.

Data and code availability

The RNA sequencing data reported in this paper are archived in SRA: PRJNA1192432.

ACKNOWLEDGMENTS

We are thankful to Prof. Robert Vignali, Dr. Devid Damiani, and Dr. Lucio Calcagnile for helpful discussions and to Dr. Maria Antonietta Calvello and Dr. Vania Liverani for technical support. We thank Mr. Stefano Guglielmo, Dr. Claudia Alia, and Dr. Nicola Origlia for advice on the functional analysis of cultured networks and Dr. Diego Vozzi of the Genomics Facility of the Istituto Italiano di Tecnologia (IIT) of Genova for support in NGS activity. The research was in part supported by the Matteo Caleo Foundation, intramural funding of IIT (S.G. and L.P.) and Scuola Normale Superiore (F.C.), the PRIN grant #2022M95RC7 from the Italian Ministry of University and Research (F.C.), and the Tuscany Health Ecosystem – THE grant from MUR (F.C. and A.D.G.).

AUTHOR CONTRIBUTIONS

F.T., L.P., and F.C. conceptualized and designed the study and wrote the manuscript. F.T. and L.I. performed the experiments. F.T. set up the strategy of screening of neural culture treatments, the 2D and 3D connectivity assays, the analysis of RNA-seq data, and the MEA recordings. L.I. set up the time-series analysis of MEA data under the advice of A.D.G.; S.G. acquired research funding. All authors discussed the results and commented on the manuscript.

DECLARATION OF INTERESTS

The authors declare no competing interests.

SUPPLEMENTAL INFORMATION

Supplemental information can be found online at https://doi.org/10.1016/j.stemcr.2024.12.002.

Received: May 23, 2024
Revised: December 4, 2024
Accepted: December 5, 2024
Published: January 9, 2025

REFERENCES

Abellán, A., Desfilis, E., and Medina, L. (2014). Combinatorial expression of Lef1, Lhx2, Lhx5, Lhx9, Lmo3, Lmo4, and Prox1 helps to identify comparable subdivisions in the developing hippocampal formation of mouse and chicken. Front. Neuroanat. *8*, 59. https://doi.org/10.3389/fnana.2014.00059.

Berns, D.S., DeNardo, L.A., Pederick, D.T., and Luo, L. (2018). Teneurin-3 controls topographic circuit assembly in the hippocampus. Nature *554*, 328–333. https://doi.org/10.1038/nature25463.

Borello, U., Cobos, I., Long, J.E., McWhirter, J.R., Murre, C., and Rubenstein, J.L.R. (2008). FGF15 promotes neurogenesis and opposes FGF8 function during neocortical development. Neural Dev. *3*, 17. https://doi.org/10.1186/1749-8104-3-17.

Cederquist, G.Y., Asciolla, J.J., Tchieu, J., Walsh, R.M., Cornacchia, D., Resh, M.D., and Studer, L. (2019). Specification of positional identity in forebrain organoids. Nat. Biotechnol. *37*, 436–444. https://doi.org/10.1038/s41587-019-0085-3.

Charlesworth, P., Cotterill, E., Morton, A., Grant, S.G.N., and Eglen, S.J. (2015). Quantitative differences in developmental profiles of spontaneous activity in cortical and hippocampal cultures. Neural Dev. *10*, 1. https://doi.org/10.1186/s13064-014-0028-0.

Creutzfeldt, O.D. (1995). The allocortex and limbic system. In Cortex Cerebri: Performance, Structural and Functional Organisation of the Cortex, O.D. Creutzfeldt, ed. (Oxford University Press).

Dias, I., Levers, M.R., Lamberti, M., Hassink, G.C., Van Wezel, R., and Le Feber, J. (2021). Consolidation of memory traces in cultured cortical networks requires low cholinergic tone, synchronized activity and high network excitability. J. Neural. Eng. *18*, 046051. https://doi.org/10.1088/1741-2552/abfb3f.

Donato, F., Jacobsen, R.I., Moser, M.-B., and Moser, E.I. (2017). Stellate cells drive maturation of the entorhinal-hippocampal circuit. Science *355*, eaai8178. https://doi.org/10.1126/science.aai8178.

Dunville, K., Tonelli, F., Novelli, E., Codino, A., Massa, V., Frontino, A.M., Galfrè, S., Biondi, F., Gustincich, S., Caleo, M., et al. (2022). Laminin 511 and WNT signalling sustain prolonged expansion of hiPSC-derived hippocampal progenitors. Development *149*, dev200353. https://doi.org/10.1242/dev.200353.

Faedo, A., Tomassy, G.S., Ruan, Y., Teichmann, H., Krauss, S., Pleasure, S.J., Tsai, S.Y., Tsai, M.-J., Studer, M., and Rubenstein, J.L.R. (2008). COUP-TFI Coordinates Cortical Patterning, Neurogenesis, and Laminar Fate and Modulates MAPK/ERK, AKT, and ß-Catenin Signaling. Cerebr. Cortex *18*, 2117–2131. https://doi.org/10.1093/cercor/bhm238.

Feng, J., Hsu, W.-H., Patterson, D., Tseng, C.-S., Hsing, H.-W., Zhuang, Z.-H., Huang, Y.-T., Faedo, A., Rubenstein, J.L., Touboul, J., and Chou, S.J. (2021). COUP-TFI specifies the medial entorhinal cortex identity and induces differential cell adhesion to determine the integrity of its boundary with neocortex. Sci. Adv. *7*, eabf6808. https://doi.org/10.1126/sciadv.abf6808.

Franjic, D., Choi, J., Skarica, M., Xu, C., Li, Q., Ma, S., Tebbenkamp, A.T.N., Santpere, G., Arellano, J.I., Gudelj, I., et al. (2020). Molecular Diversity Among Adult Human Hippocampal and Entorhinal Cells. Preprint at bioRxiv. https://doi.org/10.1101/2019.12.31.889139.

Gaspard, N., Bouschet, T., Hourez, R., Dimidschstein, J., Naeije, G., van den Ameele, J., Espuny-Camacho, I., Herpoel, A., Passante, L., Schiffmann, S.N., et al. (2008). An intrinsic mechanism of corticogenesis from embryonic stem cells. Nature *455*, 351–357. https://doi.org/10.1038/nature07287.

Griguoli, M., and Cherubini, E. (2017). Early Correlated Network Activity in the Hippocampus: Its Putative Role in Shaping

Neuronal Circuits. Front. Cell. Neurosci. *11*, 255. https://doi.org/10.3389/fncel.2017.00255.

Gu, Z., and Yakel, J.L. (2017). Inducing theta oscillations in the entorhinal hippocampal network in vitro. Brain Struct. Funct. *222*, 943–955. https://doi.org/10.1007/s00429-016-1256-3.

Gu, Z., Alexander, G.M., Dudek, S.M., and Yakel, J.L. (2017). Hippocampus and Entorhinal Cortex Recruit Cholinergic and NMDA Receptors Separately to Generate Hippocampal Theta Oscillations. Cell Rep. *21*, 3585–3595. https://doi.org/10.1016/j.celrep.2017.11.080.

Imaizumi, K., Fujimori, K., Ishii, S., Otomo, A., Hosoi, Y., Miyajima, H., Warita, H., Aoki, M., Hadano, S., Akamatsu, W., and Okano, H. (2018). Rostrocaudal Areal Patterning of Human PSC-Derived Cortical Neurons by FGF8 Signaling. eNeuro *5*. ENEURO.0368-17.2018. https://doi.org/10.1523/ENEURO.0368-17.2018.

Issa, J.B., Radvansky, B.A., Xuan, F., and Dombeck, D.A. (2024). Lateral entorhinal cortex subpopulations represent experiential epochs surrounding reward. Nat. Neurosci. *27*, 536–546. https://doi.org/10.1038/s41593-023-01557-4.

Kelava, I., and Lancaster, M.A. (2016). Stem Cell Models of Human Brain Development. Cell Stem Cell *18*, 736–748. https://doi.org/10.1016/j.stem.2016.05.022.

Kim, T.-G., Yao, R., Monnell, T., Cho, J.-H., Vasudevan, A., Koh, A., Peeyush, K.T., Moon, M., Datta, D., Bolshakov, V.Y., et al. (2014). Efficient Specification of Interneurons from Human Pluripotent Stem Cells by Dorsoventral and Rostrocaudal Modulation. Stem Cell. *32*, 1789–1804. https://doi.org/10.1002/stem.1704.

Leprince, E., Dard, R.F., Mortet, S., Filippi, C., Giorgi-Kurz, M., Bourboulou, R., Lenck-Santini, P.-P., Picardo, M.A., Bocchio, M., Baude, A., and Cossart, R. (2023). Extrinsic control of the early postnatal CA1 hippocampal circuits. Neuron *111*, 888–902.e8. https://doi.org/10.1016/j.neuron.2022.12.013.

Lodato, S., and Arlotta, P. (2015). Generating Neuronal Diversity in the Mammalian Cerebral Cortex. Annu. Rev. Cell Dev. Biol. *31*, 699–720. https://doi.org/10.1146/annurev-cellbio-100814-125353.

Malone, T.J., Tien, N.-W., Ma, Y., Cui, L., Lyu, S., Wang, G., Nguyen, D., Zhang, K., Myroshnychenko, M.V., Tyan, J., et al. (2024). A consistent map in the medial entorhinal cortex supports spatial memory. Nat. Commun. *15*, 1457. https://doi.org/10.1038/s41467-024-45853-4.

Minatohara, K., Akiyoshi, M., and Okuno, H. (2016). Role of Immediate-Early Genes in Synaptic Plasticity and Neuronal Ensembles Underlying the Memory Trace. Front. Mol. Neurosci. *8*. https://doi.org/10.3389/fnmol.2015.00078.

Nair, R.R., Blankvoort, S., Lagartos, M.J., and Kentros, C. (2020). Enhancer-Driven Gene Expression (EDGE) Enables the Generation of Viral Vectors Specific to Neuronal Subtypes. iScience *23*, 100888. https://doi.org/10.1016/j.isci.2020.100888.

Nilssen, E.S., Doan, T.P., Nigro, M.J., Ohara, S., and Witter, M.P. (2019). Neurons and networks in the entorhinal cortex: A reappraisal of the lateral and medial entorhinal subdivisions mediating parallel cortical pathways. Hippocampus *29*, 1238–1254. https://doi.org/10.1002/hipo.23145.

Puelles, L., Alonso, A., García-Calero, E., and Martínez-de-la-Torre, M. (2019). Concentric ring topology of mammalian cortical sectors and relevance for patterning studies. J. Comp. Neurol. *527*, 1731–1752. https://doi.org/10.1002/cne.24650.

Qian, X., Su, Y., Adam, C.D., Deutschmann, A.U., Pather, S.R., Goldberg, E.M., Su, K., Li, S., Lu, L., Jacob, F., et al. (2020). Sliced Human Cortical Organoids for Modeling Distinct Cortical Layer Formation. Cell Stem Cell *26*, 766–781.e9. https://doi.org/10.1016/j.stem.2020.02.002.

Ramsden, H.L., Sürmeli, G., McDonagh, S.G., and Nolan, M.F. (2015). Laminar and Dorsoventral Molecular Organization of the Medial Entorhinal Cortex Revealed by Large-scale Anatomical Analysis of Gene Expression. PLoS Comput. Biol. *11*, e1004032. https://doi.org/10.1371/journal.pcbi.1004032.

Sabatini, B.L., and Regehr, W.G. (1999). TIMING OF SYNAPTIC TRANSMISSION. Annu. Rev. Physiol. *61*, 521–542. https://doi.org/10.1146/annurev.physiol.61.1.521.

Sarkar, A., Mei, A., Paquola, A.C.M., Stern, S., Bardy, C., Klug, J.R., Kim, S., Neshat, N., Kim, H.J., Ku, M., et al. (2018). Efficient Generation of CA3 Neurons from Human Pluripotent Stem Cells Enables Modeling of Hippocampal Connectivity In Vitro. Cell Stem Cell *22*, 684–697.e9. https://doi.org/10.1016/j.stem.2018.04.009.

Sheroziya, M.G., Von Bohlen Und Halbach, O., Unsicker, K., and Egorov, A.V. (2009). Spontaneous Bursting Activity in the Developing Entorhinal Cortex. J. Neurosci. *29*, 12131–12144. https://doi.org/10.1523/JNEUROSCI.1333-09.2009.

Shipkov, D., Nasretdinov, A., Khazipov, R., and Valeeva, G. (2024). Synchronous excitation in the superficial and deep layers of the medial entorhinal cortex precedes early sharp waves in the neonatal rat hippocampus. Front. Cell. Neurosci. *18*, 1403073. https://doi.org/10.3389/fncel.2024.1403073.

Terrigno, M., Bertacchi, M., Pandolfini, L., Baumgart, M., Calvello, M., Cellerino, A., Studer, M., and Cremisi, F. (2018a). The microRNA miR-21 Is a Mediator of FGF8 Action on Cortical COUP-TFI Translation. Stem Cell Rep. *11*, 756–769. https://doi.org/10.1016/j.stemcr.2018.08.002.

Terrigno, M., Busti, I., Alia, C., Pietrasanta, M., Arisi, I., D'Onofrio, M., Caleo, M., and Cremisi, F. (2018b). Neurons Generated by Mouse ESCs with Hippocampal or Cortical Identity Display Distinct Projection Patterns When Co-transplanted in the Adult Brain. Stem Cell Rep. *10*, 1016–1029. https://doi.org/10.1016/j.stemcr.2018.01.010.

Valeeva, G., Janackova, S., Nasretdinov, A., Rychkova, V., Makarov, R., Holmes, G.L., Khazipov, R., and Lenck-Santini, P.-P. (2019). Emergence of Coordinated Activity in the Developing Entorhinal–Hippocampal Network. Cerebr. Cortex *29*, 906–920. https://doi.org/10.1093/cercor/bhy309.

Witter, M.P., Doan, T.P., Jacobsen, B., Nilssen, E.S., and Ohara, S. (2017). Architecture of the Entorhinal Cortex A Review of Entorhinal Anatomy in Rodents with Some Comparative Notes. Front. Syst. Neurosci. *11*, 46. https://doi.org/10.3389/fnsys.2017.00046.

Yu, D.X., Di Giorgio, F.P., Yao, J., Marchetto, M.C., Brennand, K., Wright, R., Mei, A., McHenry, L., Lisuk, D., Grasmick, J.M., et al. (2014). Modeling hippocampal neurogenesis using human pluripotent stem cells. Stem Cell Rep. *2*, 295–310. https://doi.org/10.1016/j.stemcr.2014.01.009.

Zilles, K. (2004). Architecture of the Human Cerebral Cortex. In The Human Nervous System (Elsevier), pp. 997–1055.